Effective SWI-based
Brain Segmentation Method in an MR Image

Sung-Jong Eun, Jeongmin Kwon, and Taeg-Keun Whangbo*

Abstract— **Object recognition is usually processed based on region segmentation algorithm. Region segmentation in the IT field is carried out by computerized processing of various input information such as brightness, shape, and pattern analysis. If the information mentioned does not make sense, however, many limitations could occur with region segmentation during computer processing. Therefore, this paper suggests effective region segmentation method based on Susceptibility Weighted Imaging (SWI) within the magnetic resonance (MR) theory. In this study, the experiment had been conducted using images including the brain region and by getting up contrast enhancement image of SWI for texture analysis to enable region (white matter) segmentation even when the border line was not clear. As a result, an average area difference of 7.6%, which was higher than the accuracy of conventional region segmentation algorithm, was obtained.**

Index Terms— **Susceptibility Weighted Imaging (SWI), Brain Segmentation, MR image, Texture Analysis, Curve Fitting**

I. INTRODUCTION

Object recognition is a very important part of image processing. It can begin with area segmentation and image segmentation, which is crucial for image interpretation and is an indispensable stage of image processing. Various image segmentation methods have different characteristics and perform differently according to the input image characteristics; but despite these differences, their image segmentation problems have the same causes. According to the distribution of neighboring pixel values, non-segmentation or excessive segmentation occur. These problems are common chronic problems with various image segmentation methods, and many studies have been conducted to resolve them.

Generally, image segmentation algorithms include the threshold value technique, the edge detection technique, region growing, and the technique of using texture characteristic values [1-4]. The threshold value method involves creating histograms for the given image, determining the critical value, and partitioning the image into the object and the background. Edge detection refers to the process of looking for gray-level discontinuous pixels in an image. Region growing [5] was designed to measure similarities between pixels to be able to expand and segment an area. In addition, the statistical method and the structural method use texture characteristic values that quantify discontinuous changes in pixel values in an image [6]. In addition to these general methods, methods of segmenting an area manually have been extensively studied, and multi-area segmentation methods are being applied [7]. Of these methods, the Graph Cut [8] method and the GrabCut [9] method of looking for borders to minimize energy have been proposed as methods of minimizing the involvement of users, but they have the disadvantage of requiring the setting of the initial area. Also, the Region Adaptive Algorithm method of extracting features by area using appropriate methods has been proposed, but it has the weakness of yielding inaccurate results in ambiguous borders. To resolve these shortcomings, the curve fitting method based on regional minimum values is being used. In addition, ACM or the snake method [10] was proposed to converge to the point where the energy value is minimum, to detect the optimal contour line. This snake method requires significant user information involvement, however, and has the problem of the misconception of the energy value in a shady area as a different area. To resolve these problems, diverse snake methods have been proposed [11-12].

Representative image segmentation algorithm stems from the difference in pixel information. The difference in pixel, which is input information, is determined by the difference in brightness or shape/pattern, which is connecting information. However, if the difference cannot be identified from the input information, the accuracy of region segmentation dramatically decreases. This paper suggests an effective segmentation method using magnetic resonance (MR) theory to resolve this problem. Magnetic resonance imaging (MRI) is an examination method that produces images using nuclear magnetic resonance (NMR). Resonance means an amplification reaction to the stimulations having with the same frequencies. NMR method measures the signals that come out from a nucleus when it is stimulated by its own characteristic frequency. Human bodies become feeble magnets in a magnetic field. Because the degree of magnetization differs according to the tissues of a human body, an MRI image can be obtained by measuring and graphing the difference through computer processing [13].

There are three types of MRI images: proton density image, T1 image, and T2 image [14-15]. This paper worked towards improving the quality of an image including the brain region, and tried to isolate the brain region (white matter) from the image using texture analysis method by setting up several region of the brain image. This method does not use the conventional pixel information for input information, but instead uses on Susceptibility Weighted Imaging (SWI) [16].

Sung-Jong Eun is with Department of Computer Science, Gachon University,Sujung-Gu, Seongnam, Gyunggi-Do, Korea (e-mail: asclephios@hotmail.com)

Jeongmin Kwon is with Department of Medical Sciences, Seoul National University, Jongno-Gu, Seoul, Korea (e-mail: victorkjm@snu.ac.kr))

Taeg-Keun Whangbo (* Corresponding author) is with Department of Computer Science, Gachon University, Sujung-Gu, Seongnam, Gyunggi-Do, Korea (e-mail: tkwhangbo@gachon.ac.kr)

SWI is a new means to enhance contrast in MR imaging [17-20]. Until recently, with the exception of phase being used for large-vessel flow quantification or for use in inversion recovery sequences, most diagnostic MR imaging relied only on the reading of magnitude information. The phase information was ignored and usually discarded before even reaching the viewing console. Phase images, however, contain a wealth of information about local susceptibility changes between tissues [21-23], which can be useful in measuring iron content and other substances that change the local field. The effects of other background magnetic fields presented a major problem by obscuring the useful phase information. Hence, for nearly 20 years, phase information in flow-compensated sequences went essentially unused as a means to measure susceptibility in clinical MR imaging. In this paper, we try to enhance the accuracy of object segmentation by using SWI process.

II. PROPOSED METHOD

Recognizing the brain region (white matter) in an MR image provides important information for deciding on therapy or operation method, as well as identifies diseases in the brain. This paper tries to enhance the accuracy of recognition by using SWI information. The proposed method works as follows: First, the SWI process in T2 image is calculated; second, the calculated each brain regions by the texture analysis method; and finally, the brain region is fitted using the curve fitting method in each T2 Slice. Figure 1 shows the general algorithm flowchart. Detailed and step-by-step explanation will be given thereafter.
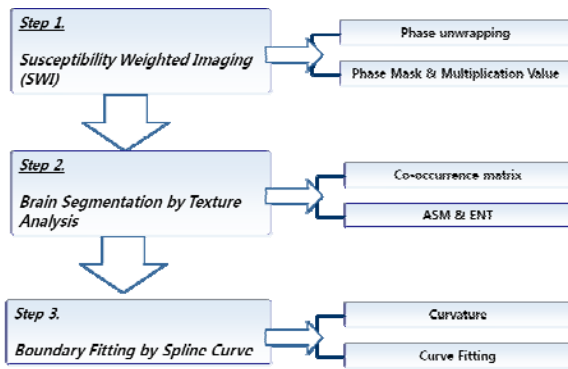

Fig. 1. Overview of the proposed method

A. Susceptibility Weighted Imaging (SWI)

SWI is a new means to enhance contrast in MR imaging. A number of important tissues have unique magnetic susceptibility differences relative to background or surrounding tissues. One such example is partially deoxygenated venous blood [23-25]. Other examples include clot(paramagnetic), calcium(diamagnetic), and iron-laden tissue [26], and air/tissue interfaces. These bulk magnetic susceptibilities are indistinguishable from chemical shift effects.

The most common example of the latter in magnetic resonance imaging (MRI) is the chemical shift difference between water and fat. Usually chemical shift effects are ignored, but in the case of water and fat separation [27-28]

the 3.35-ppm difference is used to separate water and fat. On the other hand, if information regarding several species occupying the same voxel is desired, one usually obtains the spectral information by collecting a time series of data and Fourier transforming the data. This is referred to as chemical shift imaging. Since we focus on the role of susceptibility, and use the original phase image both by itself and as a means of altering the contrast in the magnitude images, we refer to this method as SWI [16]. Although SWI has been used as an MR venographic method for several years [29], it has more recently been applied to studies of arterial venous malformations [30], occult venous disease [31], multiple sclerosis [32], trauma [33], tumors [34], and functional brain imaging [35].

Our goal in this part was to use phase to enhance contrast between tissues with different susceptibilities. All the processing steps involved in the creation of susceptibility weighted magnitude images are schematically summarized in Figure 2.
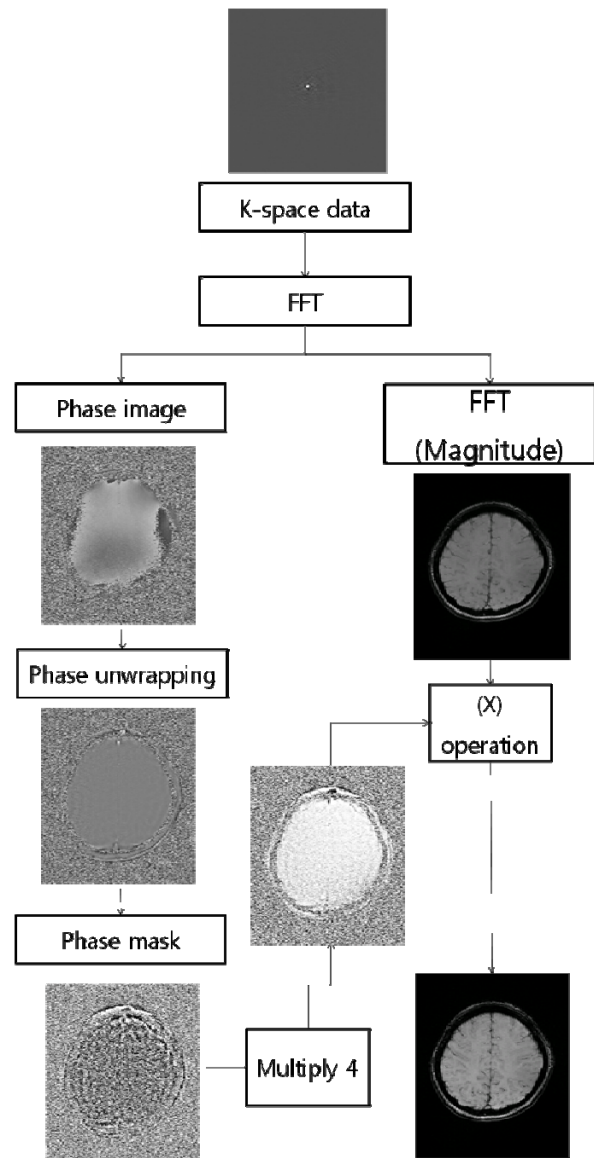

Fig. 2. The whole process of Susceptibility Weighted Imaging(SWI)

According to Figure 2, this can be accomplished in several

steps. First, we employ the high-pass filter for phase unwrapping [36], we use a 32x32 low-pass filter and divide this into the original phase image(512x512) to create a high-pass filter effect.

Second, this corrected phase image is used to create a phase mask that is used to multiply the original magnitude image to create novel contrasts in the magnitude image. The phase mask is designed to suppress those pixels that have certain phases. It is usually applied in the following manner: If the minimum phase of interest is, for example, -π, then the phase mask is designed to be f(x)(φ(x)+π)/π for phases < 0, and to be unity otherwise, where φ(x) is the phase at location x. That is, those pixels with a phase of -π will be completely suppressed and those with a value between -π and zero phase will be only partly suppressed. This phase mask (f(x)) then takes on values that lie between zero and unity. We will refer to it as the negative phase mask. It can be applied any number of times (integer m) to the original magnitude image (ρ(x)) to create a new image fm(x)ρ(x) with different contrasts[36-37]. Another mask might be defined to highlight positive phase differences by equation 1.

$$\rho(x)_{new} = g^m(x)\rho(x) \qquad (1)$$

If the maximum phase of interest is, for example, π, then the phase mask is designed to be g(x) = (π-φ(x)) / π for phase > 0, and unity otherwise. We will refer to this as the positive phase mask. And we decide the phase mask multiplication value by some experiments. So we can get the meaningful contrast enhancement image by SWI process.

B. Brain Segmentation by Texture Analysis

In this phase, the contrast quality of above enhancement result, which have previously been calculated. The candidate boundary line should be using as segmentation boundary in the third phase, which uses the texture analysis method. Detecting boundary line consists of two tasks. First is limiting the scope of detection. This requires establishing a candidate area to detect boundary line, within which the actual brain region should be detected. Second is identifying the pixels that are considered meaningful as feature points. These feature points are used as input information of the correct the boundary line, which is the next phase.

Deciding on the candidate area for boundary line is conducted through texture analysis. The texture analysis in this paper assumes that the candidate area is one that has uniform characteristics when analyzed through co-occurrence matrix [38]. Co-occurrence matrix is one of the tools used in texture imaging and is based on secondary statistical value, which represents the distribution of position pixel values of (x1, y1) and (x2, y2). If the dimension of the measured window is MxN (3x3) and the gray level is L-Level, the dimension of co-occurrence matrix C is LxL, and is calculated as following equation 2.

$$C = \{c_{m,n}\} = C_0 + C_{\pi/2} + C_\pi + C_{3\pi/2} \qquad (2)$$

C_θ is co-occurrence matrix of a coupled pixel adjacent to θ

direction. Co-occurrence matrix is used in detecting the brain region so that a region having homogeneity could be detected in a flexible way. This paper tried to find a region that shows how regularly the brightness of pixels in a window varies using Angular Second Moment (ASM). Equations 3 can be used in calculating ASM.

$$ASM : \sum_{i=0}^{N-1}\sum_{j=0}^{N-1} P_{ij}^{\ 2} \qquad (3)$$

$P_{i,j}$ is used as the weight of each pixel, and it can be said that the bigger the ASM value, the more regularly the brightness changes.

C. Boundary Fitting by Spline Curve

To find the area whose segmentation boundary must be corrected, the curvature [39] of the contour is computed based on the detected brain regions. The curvature calculation process is illustrated in the figure below, together with all the pixels whose curvature values do not coincide with the critical value as the mean.
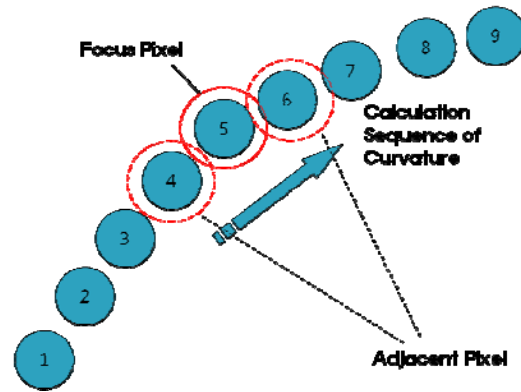

Fig. 3. Concept of curvature calculation

In Figure 3, based on pixel no. 5, the gradient difference between the neighboring pixel nos. 6 and 4 is raised to the second power, and the resulting value is divided by the Euclidean distance difference between the two pixels. Then based on a total of eight neighboring pixels (nos. 6, 4, 7, 3, 8, 2, 9, and 1), pixel no. 5's curvature is calculated. The relevant curvature calculation can be defined again by the following equation 4.

$$\begin{aligned}
&Curvature(N)\\
&= (g(N+1) - g(N-1))^2 / d((N+1) - (N-1))\\
&+ (g(N+2) - g(N-2))^2 / d((N+2) - (N-2))\\
&+ (g(N+3) - g(N-3))^2 / d((N+3) - (N-3))\\
&+ (g(N+4) - g(N-4))^2 / d((N+4) - (N-4))
\end{aligned} \qquad (4)$$

where g denotes the slope value and denotes the Euclidean distance. The next pixel's (no. 6's) curvature can likewise be calculated using pixel nos. 7, 5, 8, 4, 9, 3, 10, and 2. In this way, the curvatures of all the pixels on the peripheral line can be calculated.

Afterwards, the derived pixels are clustered. In this study, the Mean-Shift clustering [40] method was used for this purpose because the boundary of the adjacent areas was unsupervised. Where there is only one class result of clustering, it is not considered, but if there are two or more classes, the ratios between the pairs of classes are considered, and if the 7:3 ratio is exceeded, the classes of the lower ratios are adjudged meaningless. Next, all the pixels inside the finally selected class are interconnected by straight lines, and the starting and ending points of the straight lines are extracted and connected again with straight lines. Afterwards, the local minimum values of the pixels crossing at right angles are calculated based on the connected straight lines. These local minimum values are the first candidate segmentation points. The final candidate segmentation points are detected by considering the texture information of the adjacent areas of the detected first candidate points. The adjacent areas are the pixels crossing at right angles. Equation 4 shows the calculation of the entropy value, which is the texture information used.

$$ENT : \sum_{i=0}^{N-1} \sum_{j=0}^{N-1} P_{i,j}(-\ln P_{i,j}) \qquad (5)$$

$P_{i,j}$ is used as the weight of each pixel. This calculation determines the peak of the entropy value as the final candidate segmentation point.

The final candidate segmentation points are the sampling results, and curve fitting is needed to connect them. For curve fitting in this step, the boundary is created through the Catmul-Rom spline curve [41]. The boundary is finally determined through template matching. Equation 6 below shows this curve-fitting method. Lastly, the boundary is smoothened using a Median filter.

$$Q(t) = 0.5 \times (1.0f, t, t^n) \times [Mat_{n \times n}] \times [P_{n-1}] \qquad (6)$$

Given the control points P_0, P_1, P_2, and P_3 and the value t, the location of the point can be calculated. P represent the control points, t represent the signifies the portion of the distance between the two nearest control points, Mat represent the $n \times n$ matrix.

III. EXPERIMENT

To evaluate the proposed method, experiments based on medical MR imaging were performed, and the results were compared with the reference image achieved by a specialist doctor. Thus, the accuracy of the method was evaluated quantitatively. Towards this end, the difference ratio between the reference image and the area from the proposed method was calculated, and can be expressed by the following equation.

$$R_{diff} = \frac{|R_{criteria} - R_{proposed}|}{R_{criteria}} \times 100 \qquad (7)$$

In Equation 7, R_{diff} denotes the area difference ratio, $R_{criteria}$ denotes the area of the reference image, and $R_{proposed}$

represents the area created by the proposed method. For this experiment, a total of 30 MR images were processed, and the relevant image criteria were evaluated according to the results of the proposed method and of Equation 7, after a specialist doctor established the baseline using Adobe Photoshop CS. In our case, to evaluate the accuracy, we calculate the average area difference by each slice in brain volume data. As a result, an average area difference ratio of 7.6% was determined. Figure 4 shows the some samples of evaluation result in the proposed method.

To provide more points for comparison, other techniques were implemented such as the general region growing [5] and snake [10] methods using the slice 30 images in Figure 4 and Table 1 show the sample results of the application of the comparison algorithm.

Actually, proposed method is composed of general segmentation algorithm in addition to MR theory as SWI information. So that's why we choose the comparison method like a region growing and snake model. In case of region growing, seed point is set the manually by criteria boundary. Threshold value was calculated by average intensity. In case of snake model, initial contour set the manually by criteria boundary. According to the results shown in Figure 4 and Table 1, the existing snake method and region growing caused some problems in that the intensity or energy recognized portions with ambiguous shades as different areas.
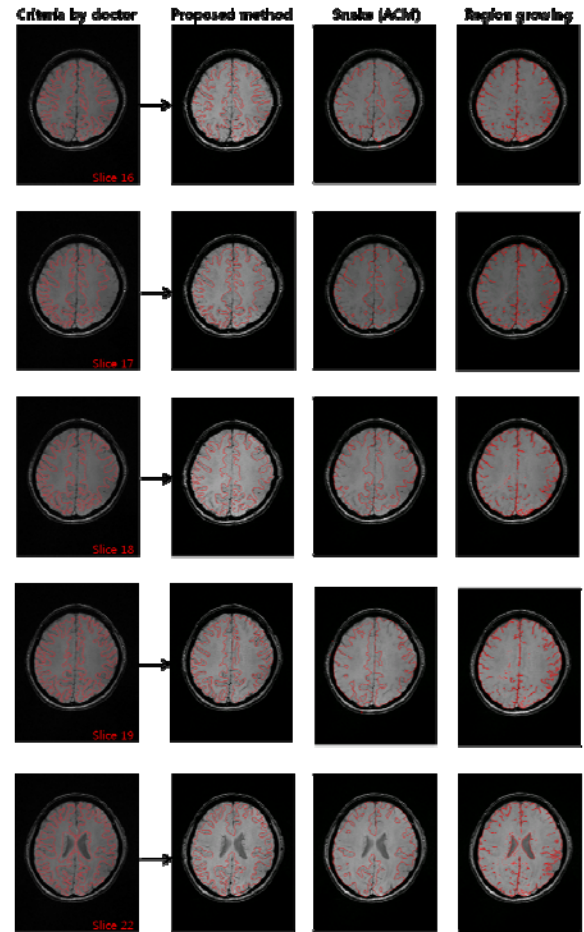

Fig. 4. The comparison samples of each final results

TABLE I
RESULTS OF COMPARISON OF THE PROPOSED METHOD
WITH THE OTHER METHODS

Method	Average area difference ratio
Region Growing	15.5%
Snake	10.2%
Proposed Method	7.6%

IV. CONCLUSION

In this paper, SWI process within the MR theory has been used to resolve the basic limitations in computer processing. It suggested detection of meaningful segmented regions. It also suggested an effective algorithm to detect the brain region using texture analysis based on SWI image. This method did not stick to fundamental brightness processing, but focused on finding the region that adjust the enhance contrast by SWI processing, considering the functional characteristics of the susceptibility. The results have confirmed that the meaningful region, which have been detected through a corresponding susceptibility, that is, the method in which the brain region detected through SWI were used was more accurate than the conventional one in which the difference of pixel information was used. However, when the SWI result has considerable noise or has been distorted from the internal region in brain, the accuracy of detection becomes low. This limitation should be complemented by further research on image improvement. This paper aimed to verify the possibility of improvement in computer processing by adopting the MR theory. Further research needs to be conducted to help in resolving the general limitations through the appropriate combination of MR theory and computer science.

ACKNOWLEDGMENT

REFERENCES

[1] S. Hemachande, A. Verma, S. Arora, and Prasanta K. Panigrahi. 2007. Locally Adaptive Block Thresholding Method with Continuity Constraint. Pattern Recognition Letters, 28, pp. 119-124.

[2] C. C. Kang and W. J. Wang. 2007. A Novel Edge Detection Method Based on Maximization of the Objective Function. Pattern Recognition, Vol. 40, No. 2, pp. 609-618.

[3] Rafael C. Gonzalez and Paul Wintz. 1993. Digital Image Processing, 3rd Ed., Addison-Wesley.

[4] Norio Baba, Norihiko Ichse, and Toshiyuki Tanaka. 1996. Image Area Extraction of Biological Objects from a Thin Section Image by Statistical Texture Analysis. Electron Microse 45, pp. 298-306.

[5] J. L Muerle and D. C.Allen. 1968. Experimental Evaluation of a Technique for Automatic Segmentation of Objects in Complex Scenes. IPPR, Thopmson.

[6] M. Unser. 1995. Texture Classification and Segmentation for Using Wavelet Frames. IEEE Trans., Vol. 4, No. 11, pp. 1549-1560.

[7] W. Li, C. Zhou, and Z. Zhang. 2004. Segmentation of the body of the tongue based on the improved snake algorithm in traditional Chinese medicine. In Proc. of the 5th World Congress on Intelligent Control and Automation, pp. 15-19.

[8] R. Zabih and V. Kolmogorov. 2004. Spatially coherent clustering using graph cuts. In Proc. of Computer Vision and Pattern Recognition, Vol. 2, pp. 437-444.

[9] C. Rother, V. Kolmogorov, and A. Blake. 2004. GrabCut: Interactive foreground extraction using iterated graph cuts. ACM Trans. Graphics, Vol. 23, No. 3, pp. 309-314.

[10] Michael Kass and Andrew Witkin. 1988. Demetri Terzopoulos Active Contour Models. International Journal of Computer Vision, Vol. 1, pp. 321-331.

[11] Eddie Y. K. Ng and Y. Chen. 2006. Segmentation of the Breast Thermogram: Improved Boundary Detection with the Modified Snake Algorithm. Journal of Mechanics in Medicine and Biology, Vol. 6, No. 2, pp. 123-136.

[12] Dong Joong Kang and In So Kweon. 1999. A fast and stable snake algorithm for medical images. Pattern Recognition Letters, Vol. 20, Issue 10, pp. 1069.

[13] R. I. Shrager, G. H. Weiss, R. G. S. Spence. NMR Biomed., 11, pp.297‐305, 1998.

[14] R.V. Damadian, Science, 171, pp.1151‐1153, 1971.

[15] R.A. de Graaf, P.B. Brown, S. McIntyre, T.W. Nixon, K.L. Behar, D.L. Rothman, Magn. Reson.Med., 56, pp.386‐394, 2006.

[16] Haacke EM, Xu Y, Cheng YC, Reichenbach JR. Susceptibility weighted imaging (SWI). Magn Reson Med 2004;52:612–618.

[17] Cheng YC, Haacke EM, Yu YJ. An exact form for the magnetic field density of states for a dipole. Magn Reson Imaging 2001;19:1017–23.

[18] Schad LR. Improved target volume characterization in stereotactic treatment planning of brain lesions by using high-resolution BOLD MR-venography.NMR Biomed 2001;14:478–83.

[19] Reichenbach JR, Haacke EM. High-resolution BOLD venographic imaging; a window into brain function. NMR Biomed 2001;14:453–67.

[20] Reichenbach JR, Jonetz-Mentzel L, Fitzek C, et al. High-resolution blood oxygen-level dependent MR venography (HRBV): a new technique. Neuroradiology 2001;43:364–69.

[21] Wang Y, Yu Y, Li D, et al. Artery and vein separation using susceptibilitydependent phase in contrast-enhanced MRA. J Magn Reson Imaging 2000;12:661–70.

[22] Fernandez-Seara MA, Techawiboonwong A, Detre JA, et al. MR susceptometry for measuring global brain oxygen extraction. Magn Reson Med 2006;55:967–73.

[23] Haacke EM, Ayaz M, Khan A, et al. Establishing a baseline phase behavior in magnetic resonance imaging to determine normal vs. abnormal iron content in the brain. J Magn Reson Imaging 2007;26:256–64.

[24] Ogawa S, Lee TM, Kay AR, Tank DW. Brain magnetic resonance imaging with contrast dependent on blood oxygenation. Proc Natl Acad SciUSA 1990;87:9868–9872.

[25] Ogawa S, Lee TM. Magnetic resonance imaging of blood vessels at high fields: in vivo and in vitro measurements and image simulation. Magn Reson Med 1990;16:9–18.

[26] Ogawa S, Lee TM, Nayak AS, Glynn P. Oxygenation-sensitive contrast in magnetic resonance image of rodent brain at high magnetic fields.Magn Reson Med 1990;14:68–78.

[27] Ogg RJ, Langston JW, Haacke EM, Steen RG, Taylor JS. The correlation between phase shifts in gradient-echo MR images and regional brain iron concentration. Magn Reson Imaging 1999;17:1141–1148.

[28] Dixon WT. Simple proton spectroscopic imaging. Radiology 1984;153:189–194.

[29] Haacke, EM, Patrick JL, Lenz GW, Parrish T. The separation of water and lipid components in the presence of field inhomogeneities. Rev Magn Reson Med 1986;1:123–154.

[30] Reichenbach JR, Essig M, Haacke EM, Lee BC, Przetak C, Kaiser WA, Schad LR. High resolution venography of the brain using magnetic resonance imaging. MAGMA 1998;6:62–69.

[31] Essig M, Reichenbach JR, Schad LR, Scho¨nberg SO, Debus J, Kaiser WA. High-resolution MR venography of cerebral arteriovenous malformations.Magn Reson Imaging 1999;17:1417–1425.

[32] Lee BCP, Vo KD, Kido DK, Mukherjee P, Reichenbach J, Lin W, Yoon MS, Haacke EM. MR high-resolution blood oxygenation level-dependent venography of occult (low-flow) vascular lesions. AJNR Am J Neuroradiol 1999;20:1239–1242.

[33] Tan IL, van Schijndel RA, Pouwels PJW, van Walderveen MAA,Reichenbach JR, Manoliu RA, Barkhof F. MR venography of multiple sclerosis. AJNR Am J Neuroradiol 2000;21:1039–1042.

[34] Tong KA, Ashwal S, Holshouser BA, Shutter L, Herigault G, Haacke EM, Kido DK. Improved detection of hemorrhagic shearing lesions in children with post-traumatic diffuse axonal injury—initial results. Radiology 2003;227:332–339.

[35] Reichenbach JR, Jonetz-Mentzel L, Fitzek C, Haacke EM, Kido DK, Lee BCP, Kaiser WA. High-resolution blood oxygen-level dependent MR venography (HRBV): a new technique. Neuroradiology 2001;43:364–369.

[36] Baudendistel KT, Reichenbach JR, Metzner R, Schro¨der J, Schad LR. Comparison of functional venography and EPI-BOLD-fMRI at 1.5T.Magn Reson Imaging 1998;16:989–991.

[37] Reichenbach JR, Venkatesan R, Schillinger DJ, Kido DK, Haacke EM.Small vessels in the human brain: MR venography with deoxyhemoglobin as an intrinsic contrast agent. Radiology 1997;204:272–277.

[38] B.Chande and D.Dutta Majumder, "A note on the graylevel co-occurrence matrix in threshold selection", Signal Processing, vol. 15, no. 2, Sep 1988

[39] Murphy, T. M., Math, M. and Finke, L. H., "Curvature Covariation as a Factor of Perceptual Salience," International IEEE EMBS CNECI, pp. 16-19, 2003.

[40] Comaniciu, D. and Meer, P., "Mean Shift Analysis and Application," Seventh Int'IConf. Computer Vision and Pattern Recognition, pp.750-755, 1997

[41] Catmull, E. and Rom, R., "A class of local interpolating splines," Computer Aided Geometric Design, pp. 317-326, 1974